**Atmospheric
Chemistry
and Physics
Discussions**

The impact of soil uptake on the global distribution of molecular hydrogen: chemical transport model simulation

H. Yashiro[1], K. Sudo[1,2], S. Yonemura[3], and M. Takigawa[1]

[1]Research Institute for Global Change, Japan Agency for Marine-Earth Science and Technology, Yokohama, Japan
[2]Graduate School of Environmental Studies, Nagoya University, Nagoya, Japan
[3]National Institute for Agro-Environmental Sciences, Tsukuba, Japan

Correspondence to: H. Yashiro (h.yashiro@jamstec.go.jp)

ACPD

11, 4059–4103, 2011

Chemical transport model simulation

H. Yashiro et al.

Title Page

Abstract	Introduction
Conclusions	References
Tables	Figures

|◄   ►|

◄   ►

Back   Close

Full Screen / Esc

Printer-friendly Version

Interactive Discussion

Abstract

The molecular hydrogen (H_2) in the troposphere is highly influenced by the strength of H_2 uptake by the terrestrial soil surface. The global distribution of H_2 and its uptake by the soil are simulated by using a model called CHemical AGCM for Study of Environment and Radiative forcing (CHASER), which incorporates a 2-layered soil diffusion/uptake process component. The simulated distribution of deposition velocity over land reflects regional climate and has a global average of $3.3 \times 10^{-2}\,\mathrm{cm\,s^{-1}}$. In the region north of 30° N, the amount of soil uptake increases, particularly in the summer. However, the increase in the uptake becomes smaller in the winter season due to snow cover and a reduction in the biological activity at low temperatures. In the temperate and humid regions in the mid- and low-latitudes, the uptake is mostly influenced by the soil air ratio, which controls the gas diffusivity in the soil. In the semi-arid region, water stress and high temperature contribute to the reduction of biological activity, as well as to the seasonal variation in the deposition velocity. The comparison with the observations shows that the model reproduces both the distribution and seasonal variation of H_2 relatively well. The global burden and tropospheric lifetime are 150 Tg and 2.0 yr, respectively. The seasonal variation of H_2 in the northern high latitude is mainly controlled by the large seasonal change in soil uptake. In the Southern Hemisphere, the seasonal change in the net chemical production and inter-hemispheric transport are the dominant cause of the seasonal cycle. Large biomass burning impacts the magnitude of seasonal variation mainly in the tropics and subtropics. Both observation and model show large inter-annual variation, especially for the period 1997–1998, associated with the large biomass burning in tropics and northern high-latitudes. The soil uptake shows relatively small inter-annual variability compared to the signal from biomass burning. We note that the thickness of biologically inactive layer near the soil surface and the uptake flux in semi-arid region is important for the current and future budget of atmospheric H_2.

1 Introduction

In the troposphere, molecular hydrogen (H_2) has an average concentration of ~530 ppb, the second highest after methane (CH_4, ~1750 ppb) in the reactive tracers. Its lifetime (~2 yr) is shorter than CH_4 (~9–11 yr) and longer than carbon monoxide (CO, ~3 months) (see Ehhalt and Rohrer, 2009 and references therein). Although many of the anthropogenic sources are distributed over the land surface in the Northern Hemisphere, ground and airborne observations show that the atmospheric H_2 shows the lowest concentrations in mid- and high- latitude regions near the surface in the Northern Hemisphere (Novelli et al., 1999). H_2 increases towards the tropics, becoming relatively uniform in distribution with latitude in the Southern Hemisphere. This distribution differs from those of other trace gases like CO_2, CH_4 and chlorofluorocarbons. It is interesting to note that, although the tropospheric sources of CO and H_2 are similar, their latitudinal distribution and seasonal variation are different. One reason for this is that one of the major factors contributing to the observed spatio-temporal distribution of H_2 is soil uptake, which makes up about 75–82% of the sink. H_2 is produced from formaldehyde (HCHO) in the atmosphere through the chemical reaction process that begins from oxidization of CH_4 or non-methane volatile organic compounds (NMVOCs). Moreover, H_2 is oxidized by a reaction with OH. H_2 is thus continuously generated in the troposphere and is removed by soil or is exchanged with the stratosphere.

The H_2 emissions from fossil fuel consumption and industrial activities have been increasing since the beginning of the industrial era. It is likely that when the humans shift to the "hydrogen-economy" society, with hydrogen as a secondary energy source, a large amount of H_2 could leak into the atmosphere. Some studies have shown that an increasing H_2 concentration reduces the atmospheric oxidization capacity, and influences the temperature and ozone loss in the stratosphere through the production of water vapor (Prather et al., 2003; Schultz et al., 2003; Tromp et al., 2003; Warwick et al., 2004).

Although the soil uptake of H_2 is hugely important in the global H_2 cycle, we have a limited understanding of the uptake process which results in large uncertainties associated with the global distribution and seasonal variation of the soil H_2 uptake. Absorption of H_2 in the soil is mainly performed by several types of the extracellular enzymes (hy-
5   drogenase) which are believed to exist universally in the land soil (Conrad et al., 1983). Previous studies show that almost all absorption is performed in the thin soil layer near the surface (Yonemura et al., 1999). The soil temperature and soil moisture mainly control the biological activity, while snow, heated land surface and litter function as a diffusion barrier (Yonemura et al., 1999, 2000a, 2000b; Smith-Downey et al., 2006,
10 2008; Shumitt et al., 2009).

Global simulations of the H_2 concentration and its isotope composition have been conducted in previous studies. Hauglusteine and Ehhalt (2002) used a chemical transport model to show a good agreement between the observed and simulated concentration in the Southern Hemisphere and the tropics, but reported overestimation of sea-
15 sonal maximum in the Northern Hemisphere that resulted from their estimation of the soil uptake flux based on the distribution and seasonal variation of net primary productivity (NPP). Sanderson et al. (2003) used a Lagrangian model to simulate the spatial and temporal variation of deposition velocity, which depends on the vegetation type, snow cover, and soil moisture. Their model reproduced the observed seasonal varia-
20 tion at stations fairy well. Price et al. (2007) also used deposition velocity as a function of snow cover and soil temperature, to reproduce relatively well latitudinal and seasonal variations of H_2 concentration and its isotope ratio. They obtained an annual soil uptake of 50–60 Tg. The deposition velocities were constrained by the observations, and the soil uptake was empirically based, without explicitly taking into consideration
25 the actual soil uptake process. There have also been other studies that used top down approaches, resulting in larger estimated soil uptake (Rhee et al., 2006; Xiao et al., 2007).

In this study, we use a global chemistry transport model combined with land process model that includes explicit soil uptake process, to calculate the deposition flux and

concentration of H_2, and discuss the spatial and temporal variations and the global budget of H_2 in the troposphere.

2 Model description

2.1 Global chemical transport model and land process model

5　CHASER is a three-dimensional atmospheric chemical climate/transport model, which has been developed in the framework of an AGCM developed by the Center for Climate System Research (CCSR), the National Institute for Environment Studies (NIES), and the Frontier Research Center for Global Change (FRCGC). The details of the model are described in Sudo et al. (2002a, 2007) and an evaluation of the model performance
10　shows good agreements between the model simulations and observations for O_3 and its precursor species (Sudo et al., 2002b). The model performance is also evaluated in the framework of the 4th assessment report of the Intergovernmental Panel on Climate Change (IPCC) (e.g., Shindell et al., 2005; van Noije et al., 2006). The CHASER model adopted in this study includes several improvements; the model is based on the
15　new version of CCSR/NIES/FRCGC AGCM (Watanabe et al., 2008) developed as the atmospheric component of MIROC (Model for Interdisciplinary Research on Climate) (K-1 developers, 2004). In the new version of AGCM, the σ vertical coordinate system has been replaced by a hybrid σ-pressure vertical coordinate system. The updated radiation scheme by Sekiguchi and Nakajima (2009) has been adopted. A non-local
20　turbulence closure scheme based on Holtslag and Boville (1993) is applied to sub-grid transport of tracers due to turbulent mixing in conjunction with the Mellor-Yamada level 2 scheme. For this study, the horizontal resolution of T42 ($2.8° \times 2.8°$) is adopted with 32 vertical layers from the surface to about 40 km altitude ($\sim$1 km vertical resolution in the upper troposphere and lower stratosphere). In order to reduce model bias and
25　to obtain realistic meteorological fields for the period 1989–2006, the horizontal wind and temperature fields are nudged to the JRA-25 reanalysis data (Onogi et al., 2005).

Full Screen / Esc

Printer-friendly Version

Interactive Discussion

The relaxation time is optimized and set to 1 day for horizontal wind and 5 days for temperature, in accordance to Miyazaki et al. (2005).

The model considers a detailed online simulation of tropospheric chemistry involving O_3-HO_x-NO_x-CH_4-CO system and oxidation of NMVOCs with a timestep of 10 min, and includes detailed dry and wet deposition schemes. Oxidation of CH_4 and NMVOCs constitute a large source of H_2 in the model, with photolysis of HCHO leading to the formation of H_2. Details of the chemical reaction system is described in Sudo et al. (2002a), to which we add reaction of H_2 with the OH radical,

$$H_2 + OH \rightarrow H_2O + H \tag{1}$$
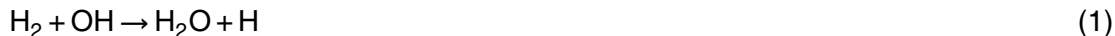
for the chemical destruction of H_2 by the OH radical, with the rate constant of $k_{H_2+OH}(T) = 7.7 \times 10^{-12} \times \exp(-2100/T)$ molecules^{-1} cm^{-3} s^{-1} (Atkinson et al., 2004).

In this study, surface emissions for CO, NO_x, CH_4, NMVOCs, SO_2 and dimethyl sulfide are included in CHASER. Other modifications made to the model as described in Sudo et al. (2002a, 2007) for the present study are as follows. Anthropogenic emissions of CO, NO_x, CH_4 and SO_2 are based on the EDGAR v3.2 1990, 1995 and "Fast-Track" 2000 (Olivier et al., 2005). The source strength at each model grid from 1990 to 2005 is obtained by linearly interpolating and extrapolating the 1990, 1995, and 2000 values. After 2005, the same source strength as for 2005 is applied. For CO and NO_x emissions from China, we switch from the EDGAR inventory to REAS v1.1 for the period 1989 to 2006 (Ohara et al., 2007). For CO, NO_x, CH_4, NMVOCs and SO_2 emissions from biomass burning, we adopt GFED v2.1 (van der Werf et al., 2006). Monthly averaged values of these emissions are assigned for the period 1997–2000, while 8-day average values are used after 2001. The values before 1997 for each selected source region were assumed to be constant in this study at a median value of the 1997–2007 monthly CO emissions. For the biogenic emissions of NMVOCs, the monthly emission data by Guenther et al. (1995), which can be obtained from the Global Emissions Inventory Activity (GEIA) database, are used with the amount of 420, 106 and 70 TgC yr^{-1} for C_5H_8, $C_{10}H_{16}$ and CH_3OH, respectively. For the other CO

emission, monthly distributions of biogenic and oceanic CO emission given by Muller et al. (1992) are used. The global source strength of biogenic CO emission is set to $160 \, \text{Tg yr}^{-1}$ and that of oceanic emission is scaled to $10 \, \text{Tg yr}^{-1}$. Emissions of NMVOCs from the ocean are adopted with the same distribution as oceanic CO emission.

5   There are few global emission inventories that do focus on H_2. For anthropogenic emission, the surface source distribution of H_2 in this study is determined by applying the H_2/CO emission ratio to the emission inventory of CO. Ehhalt and Rohrer (2009) summarized the observational results of the H_2/CO ratio and estimated an H_2/CO ratio of $0.5 \pm 0.1 \, \text{mol mol}^{-1}$ and $0.2 \pm 0.15 \, \text{mol mol}^{-1}$ for automobiles and the industrial sec-
10 tor, respectively. We apply these emission ratios and $0.32 \, \text{mol mol}^{-1}$ for biofuel combustion (Andreae and Merlet, 2001) to the EDGAR and REAS inventory. GFED v2.1 is used for the H_2 emissions from biomass burning. Large uncertainties still remain in the H_2 emission estimates for land and ocean as a by-product of the biogenic nitrogen fixation. But based on the detailed discussion and estimation in Ehhalt and Rohrer (2009),
15 we employ $3 \, \text{Tg yr}^{-1}$ and $6 \, \text{Tg yr}^{-1}$ for land and ocean emissions, respectively. The spatial and temporal distributions of these emission estimates are based on the distribution of biogenic and oceanic CO emissions. It is important to note that the enzyme involved in the H_2 production (nitrogenase) responsible for soil biogenic emissions of H_2 is different from the enzyme involved in the H_2 consumption (hydrogenase) responsible for
20 soil H_2 uptake (Conrad, 1985).

MATSIRO (Minimal Advanced Treatment of Surface Interaction and RunOff) (Takata et al., 2005) is employed as the land surface process model for the CCSR/NIES/FRCGC AGCM. The model calculates water and energy exchange between land and atmosphere based on a set of defined 10 vegetation and 8 soil types.
25 The soil is vertically resolved by 5 layers with a thickness of 5, 20, 75, 100 and 200 cm for each layer starting from the surface, with soil temperature and moisture calculated in each layer. The surface fluxes are calculated in the snow-free and snow-covered portions separately in each grid. An evaluation of MATSIRO shows that the model reproduces realistically the distributions of observed soil temperature, soil moisture,

snow cover and precipitation (Koster et al., 2004; Hirabayashi et al., 2005). By coupling CHASER and MATSIRO in the framework of MIROC, we modified the dry deposition scheme used in CHASER. The stomatal conductance for each chemical tracer is calculated by using the simulated strength of photosynthesis in MATSIRO, which is based on SiB2 (Sellers et al., 1996) and a Farquhar type formulation (Farquhar et al., 1980). A new deposition pathway related to biological consumption is described below.

2.2 Soil uptake model

The largest sink of tropospheric H_2 is uptake in the soil. H_2 consumption by soil was thought to be mainly due to kinds of abiontic enzymes (Conrad and Seiler, 1985; Conrad, 1996). Recent studies suggest that many kinds of bacteria can oxidize and consume H_2 without enzymes, such as actinobacterias, for example (Constant et al., 2010). Therefore, molecular diffusion (physical process) and enzyme/bacterial activity (biological process) determine the strength of the H_2 uptake by the soil. The intensity of the biological activity is controlled to a large extent by the soil temperature. Smith-Downey et al. (2006) showed that an enzymatic optimal activity is achieved between 20° and 30 °C, and decreases with decreasing temperature below ~10 °C. Considerable activity remains at the subzero temperature (0 to −4 °C) but there is almost no uptake below −20 °C. They also showed reduced activity over the 40 °C to 60 °C range in an experiment conducted with soils from a California forest. In addition to the temperature effect, the biological activity is also influenced by the soil moisture content, becoming less active when soil is arid or frozen. On the other hand, too much soil water reduces the porosity in the soil and restricts the diffusion of H_2 into the soil. Much of the hydrogen in the soil is consumed at depths several centimeters below the surface, i.e. below a thin inert layer near the surface (Yonemura et al., 2000b; Shumitt et al., 2009). The inactive layer acts as a diffusion barrier, and is probably caused by the dryness and high-temperature near the ground surface. Yonemura et al. (2000a) calculated the deposition velocity of H_2 using a 2-layer diffusion model that incorporated the biologically inactive and active layer. Their model was able to capture the observed vertical profiles

of H_2 in the soil and showed that the thickness of the inactive layer is important for a realistic simulation of the flux strength. In this study, we incorporate the same type of 1-D diffusion model described in Yonemura et al. (2000a) to the deposition scheme of the CHASER model.

2.2.1 General approaches of dry deposition in the model

The dry deposition scheme used in the CHASER model is mainly based on the method of Wesely (1989). The deposition flux to the canopy, the soil, the snow, and sea surface of each gas is described as follows by using a deposition velocity V_d $(m\,s^{-1})$.

$$F = -V_d \times C \qquad (2)$$

where F is the flux of the each gas $(kg\,m^{-2}\,s^{-1})$ and C is the concentration of each gas $(kg\,kg^{-1})$. V_d is expressed with the reciprocal number R $(s\,m^{-1})$ using analogy of an electrical resistance circuit. R is described as a total of the resistance as follows;

$$R = R_a + R_b + R_c \qquad (3)$$

where R_a is the aerodynamic resistance, R_b is the quasi-laminar (boundary layer) resistance, and R_c is the resistance to the uptake by canopy or ground surface. Furthermore, R_c is described as a parallel connection of the resistance according to the condition of the canopy/ground surface. Wesely (1989) expressed the difference of the surface resistance for each gas by considering the water solubility and oxidizing capacity. In this study, we calculate the deposition flux by adding a resistance term in a parallel pathway to the soil surface, R_{enz}, to R_c. R_{enz} is calculated by the soil diffusion/uptake model described below. This 1-D model has two layers in the uppermost layer of the soil. For the small solubility of H_2, we ignore the deposition of H_2 to snow and the ocean surface, and ignore the deposition to soil through snow because of the lower permeability of snow. The land process model calculates the amount of snow on the ground as a function of snowfall calculated by the atmosphere model. Deposition

Title Page

Abstract | Introduction

Conclusions | References

Tables | Figures

⏮ | ⏭

◀ | ▶

Back | Close

Full Screen / Esc

Printer-friendly Version

Interactive Discussion

of each gas onto the soil and snow surface is distributed according to the presumed rate of snow cover, which is calculated from the depth of snow on the ground.

2.2.2 Two-layered diffusion/uptake model

We now carry out an analysis of the 1-D molecular diffusion model, which has a depth-dependent uptake ratio. The deposition velocity on the soil surface, which is the inverse of the resistance except the aerodynamic and quasi-laminar resistance, is given as follows;

$$V_{dsoil} = \frac{F(z)}{\rho C(z)}, \ z = 0 \tag{4}$$

where $F(z)$ is the flux ($kg\,m^2\,s^{-1}$), ρ is the atmospheric density ($kg\,m^{-3}$), and $C(z)$ is the mass concentration of H_2 ($kg\,kg^{-1}$). z (m) is positive in the downward direction from the surface ($z = 0$), as is F. The uptake flux is written as Fick's Law and the mass balance of H_2 is expressed as follows;

$$F(z) = -Ds \times \frac{\partial \rho C(z)}{\partial z} \tag{5}$$

$$\frac{\partial \rho C(z)}{\partial t} = \frac{\partial}{\partial z}(Ds \times \frac{\partial \rho C(z)}{\partial z}) - k \times \rho \Theta C(z) \tag{6}$$

where Θ is the volume of gas per unit volume of soil (air ratio, $m\,m^{-1}$), Ds is the diffusivity in the soil driven by molecular diffusion ($m^2\,s^{-1}$), and k is the biological uptake rate in the soil (s^{-1}). In our model, we assume ρ, Θ, and Ds to be uniform from the soil surface to a sufficient depth. In addition, we include an inactive layer near the surface where no biological activity takes place. We adopt a simplified distribution of biological activity $k(z)$ as;

$$k(z) = 0 \text{ at } 0 < z < \delta \tag{7}$$

$$k(z) = k_0 \text{ at } \delta < z \tag{8}$$

where k_0 is the uptake rate (s^{-1}), a constant value below δ (m) within the uppermost layer of the soil. Since the H$_2$ uptake is relatively fast and occurs in the top soil, we assume steady state. We define the H$_2$ concentration at depth $z = 0$ as C_a and $z = \delta$ as C_δ. The concentration in the inactive layer $C_{il}(z)$ can be solved using Eqs. (6), (7), and the boundary condition:

$$C_{il}(z) = \frac{C_\delta - C_a}{\delta} z + C_a \tag{9}$$

The concentration in the active layer $C_{al}(z)$ also can solved using Eq. (6), $C_{al}(z = \delta) = C_\delta$, and $C_{al}(z = \infty) = 0$ by

$$C_{al}(z) = \frac{C_\delta}{e^{-f}} \times e^{\left(-\frac{f}{\delta}z\right)} \tag{10}$$

where $f = \delta \sqrt{\frac{k}{Ds}}$. With the condition that the flux in the boundary $F(z = \delta)$ between the two layers in the soil is equal, C_δ can be given using Eqs. (5),(9), (10) as

$$C_\delta = \frac{1}{1 + f} C_a. \tag{11}$$

The deposition velocity on the surface of the inactive layer is given by

$$\begin{aligned} V_{dsoil} &= \frac{1}{1+f} \Theta \sqrt{kDs} \\ &= \frac{\Theta Ds \sqrt{k}}{\sqrt{Ds} + \delta \sqrt{k}} \end{aligned} \tag{12}$$

Equation (12) shows that f, and thus the thickness of the inactive layer δ, is an important parameter in the reduction of the soil uptake flux. When the diffusivity in the soil is increased, the effect of the inactive layer becomes weaker. On the other hand, the biological activity does not reduce the influence of the inactive layer, and the rate restricted by the inactive layer becomes large as the activity becomes high.

The gas diffusion in the soil airspace is assumed to be driven by molecular diffusion. The soil gas diffusivity Ds can be expressed as an approximation using Millington-Quirk Model (Millington and Quirk, 1959) as follows;

$$Ds = Da \frac{\Theta^{3.1}}{\Theta_{sat}^2} \tag{13}$$

where Da is the molecular diffusion coefficient of each gas in the atmosphere, and Θ_{sat} is the maximum aerial volume per unit volume of soil. In the land process model, the solid ratio of the soil is given for each soil type in each grid and the presence of liquid water and ice limits the diffusion of the gas in the soil. The biological uptake rate will be determined not only by the degree of activity of each enzyme but also by the amount of enzyme present. However, global distributions of the H_2-comsumption enzymes/bacteria have yet to be elucidated quantitatively. For example, Smith-Downey et al. (2006) showed that a fresh litter on forest floor prevents efficient absorption of H_2 by the soil. Also the amount of organic matter and pH of the soil influence the amount of the enzyme, but previous investigations have shown that these do not appear to moderate the activity greatly (Smith-Downey et al., 2008). In this study, we model the variation of the biological activity as a function of soil temperature and moisture, in accordance with the relationship obtained by Smith-Downey (2006) and Smith-Downey et al. (2006).

$$k_0 = k_{max} \times f(T) \times f(\Theta) \tag{14}$$

$$f(T) = \frac{1}{1 + \exp(-0.1718 \times T + 46.938)} \tag{15}$$

$$f(M) = \begin{cases} 1 & M > 0.15 \\ 14.3M - 1.14 & 0.15 \geq M \geq 0.08 \\ 0 & M < 0.08 \end{cases} \tag{16}$$

$$M = \frac{\Theta_w}{\Theta_{sat}} \tag{17}$$

Printer-friendly Version

Interactive Discussion

where k_{max} is the maximum uptake rate and is assigned a value of $0.1227\,s^{-1}$ estimated by Smith-Downey (2006). M is the ratio of liquid water volume per unit volume of soil to Θ_{sat}. In our model, the soil temperature T (K) and moisture is obtained from the uppermost soil layer for the calculation of k_0.

5   As mentioned above, the inactive layer thickness δ is an influential model parameter but its global distribution is not well known. Yonemura et al. (2000b) suggested δ in a range of 0–1 centimeters from their experimental result. Schmitt et al. (2009) estimated δ to be around 0.7 cm, with a range of 0.3–1.8 cm, based on the observation at a site in Heidelberg. In this study, we use uniform δ of 0.7 cm, which is selected to obtain
10   the agreement with the global observational results (see Sect. 3 below). In addition, we double the value of δ for a week during model integration in the area where the maximum daytime land skin temperature exceeds 40 °C, to reflect the thickening effect of the inert layer under severe temperature conditions.

3   Results and discussion

15   ### 3.1   Deposition velocity and soil uptake of H_2

The distribution of the calculated surface deposition velocity of H_2, the diffusivity in the soil, and the uptake rate of enzyme activity for January and July are shown in Fig. 1. The globally-averaged deposition velocity over the land surface is $0.33 \times 10^{-2}\,cm\,s^{-1}$ for the period 1997–2005. The simulated deposition velocity shows a clear geograph-
20   ical distribution and temporal variation. For regions north of 45° N, a large seasonal change in the deposition velocity can be seen. During the winter, snow cover suppresses the soil absorption. Furthermore, the decrease of the biological activity by low temperature reduces the rate of deposition. Although the enzyme activity is still maintained near the freezing point, the biological activity in areas like Siberia stops
25   when the soil temperature falls below –25 °C because freezing of soil moisture also results in a significant reduction in enzyme activity. With the arrival of boreal spring, the

deposition velocity starts to increase and the uptake region rapidly expands to north of 50° N as soil temperature increases and ground snow melts. The deposition velocity in this region reaches a maximum during July and August, and then starts to decrease with the coming of the autumn and winter seasons. In several parts of the region north

5 of 45° N, the increase in the deposition velocity during the spring and summer is interrupted by increases in the soil moisture caused by spring snowmelt and melting soil ice in summer, reducing gas diffusivity in the soil.

In the latitude zone around 30° N, the temperature is sufficiently high for enzyme/bacteria to be active through the year and the soil moisture becomes more im-

10 portant in controlling the deposition velocity. In a desert area, the deposition velocity is near zero because of the near absence of biological activities. The semi-arid region like Central Asia or the central part of North American continent shows larger deposition velocity during the winter than during the summer. Dryness makes diffusion in the soil more efficient in taking H_2 in this area. However, for intensely high temperature

15 and dryness in the summer, the biological activity becomes weaker and soil uptake is suppressed. The temperate and humid areas such as south China and the southeastern part of North America have neither water stress nor high temperature stress, but the high soil moisture suppresses the gas diffusion in the soil.

The seasonal variation in the deposition velocity in the tropics and on the Southern

20 Hemisphere has a smaller amplitude. The factor that has a major influence on the deposition velocity in regions 20° N to 30° S is the amount of soil moisture; therefore, the spatial change in the deposition strength is connected with the shift between the rainy and dry seasons. Southern high latitude regions do not make significant contributions to the H_2 uptake because of the small soil surface area, and needless to say, Antarctica

25 is mostly covered by snow and exhibits almost no deposition.

Regional and seasonal changes in the soil uptake rates have been reported by some field observations. (See the summarized list in Ehhalt and Rohrer (2009), Table 6). Although the coarseness of the model grid resolution makes it difficult to make a direct comparison between the simulated and observed deposition velocities, we can perform

a rough comparison if the point observation is representative of a larger region. Conrad and Seiler (1980) conducted a year-round observation on the grassland near Mainz, Germany from 1978 to 1979. They reported a seasonal variation in the deposition velocity in the range of 2.6 to $8.8 \times 10^{-2}\,\mathrm{cm\,s^{-1}}$ with a maximum between May and October and a minimum between December and February. Similar results were obtained from observations made at grasslands or cultivated lands near their site. In order to compare our model value with their observed value, we choose a grid point that spatially corresponds nearly to their cultivated land. For the period between November and April, the simulated deposition velocity of $\sim 5 \times 10^{-2}\,\mathrm{cm\,s^{-1}}$ agrees with the observational results. During the warm season, the calculated deposition velocity has a large variation in the range of $5\text{–}10 \times 10^{-2}\,\mathrm{cm\,s^{-1}}$ that is associated with the diurnal variation in soil moisture and is comparable with the range of observed values. The deposition velocity observed by Smith-Downey et al. (2006) for the desert shrub of Southern California showed a steep seasonal change. The model is able to capture a similar variation in the semi-arid ecosystem region of the southwestern North America. Both the observed and modeled deposition velocities reach a maximum in early spring with a value of $\sim 9 \times 10^{-2}\,\mathrm{cm\,s^{-1}}$, falling thereafter to a value of $2\text{–}4 \times 10^{-2}\,\mathrm{cm\,s^{-1}}$ in June. The rapid decrease is caused by the water stress on the biological activity. In the northern high-latitudes, the observation at a forest site in Finland by Lallo et al. (2006) showed low deposition velocity values ($0\text{–}4 \times 10^{-2}\,\mathrm{cm\,s^{-1}}$) in winter and high values ($4\text{–}7 \times 10^{-2}\,\mathrm{cm\,s^{-1}}$) in snow-free seasons. Our model simulation agrees relatively well with the observation, producing a seasonal cycle with an amplitude range of $0\text{–}6 \times 10^{-2}\,\mathrm{cm\,s^{-1}}$. Yonemura et al. (2000b) performed a year-round observation in Asian region. They showed the deposition velocity in the range of $0\text{–}10 \times 10^{-2}\,\mathrm{cm\,s^{-1}}$ at the arable field in Japan. However, the model did not capture the seasonal cycle with the constant value of $2 \times 10^{-2}\,\mathrm{cm\,s^{-1}}$, caused by the coarse grid around Japan Island.

The seasonal variations of the soil uptake flux for five latitudinal bands are shown in Fig. 2. North of 45° N (HNH), the averaged H_2 uptake flux has a broad maximum of 21–24 Tg yr^{-1} during the period between June and August. In September, the flux begins

Printer-friendly Version

Interactive Discussion

to decrease and reaches a value of $\sim$5 Tg yr^{-1} in January. From March to May, a rapid increase of the flux is seen. In the latitude between 15° N and 45° N (LNH), the flux remains relatively high throughout the year, increasing from 15 Tg yr^{-1} in February to 20 Tg yr^{-1} in May, and then decreasing gradually thereafter to December. In the tropics (TP), the flux shows almost constant value of 15 Tg yr^{-1} during the year. In latitudes between 15° S and 45° S (LSH), the flux has small seasonal variation. The maximum and minimum values are 11 and 10 Tg yr^{-1} in austral winter and summer, respectively. Almost no uptake is seen south of 45° S due to the lack of snow-free land surface. In LNH and LSH, variation in the soil moisture is the dominant factor that governs the deposition velocity and the soil uptake. The soil moisture is controlled by rainfall associated with synoptic systems, producing relatively large day-to-day variations in the uptake flux.

3.2 Comparison with the observed H_2 concentration

We compare the simulated H_2 concentration with the observation obtained from the NOAA/Earth System Research Laboratory (ESRL) network. The summary of model-observation comparisons is given in Table 1 with an explanation of the abbreviated name of each station. The time series of observed and calculated H_2 concentration for 10 selected stations are shown in Fig. 3. The observed values of some sites indicate a large decrease in concentration from 1991 to 1993 (not shown). Previous studies on CH_4 and CO pointed to the fact that the variation during this period could be partly attributable to the effects of the Mt. Pinatubo eruption in June 1991. Our model does not consider the effect of Mt. Pinatubo and no large inter-annual variation is reproduced by the model for this period. Furthermore, our model uses the climatology for the biomass burning emission before 1996, resulting in some discrepancies with the observation. We therefore we focus our comparison for the period between 1997 and 2005. To extract the annual average, the averaged seasonal cycle, and the long-term variation, we calculate the best-fitted curve to the data using the method of Nakazawa et al. (1997).

Title Page

Abstract | Introduction

Conclusions | References

Tables | Figures

◄ | ►

◄ | ►

Back | Close

Full Screen / Esc

Printer-friendly Version

Interactive Discussion

In general, the model reproduces the observed H_2 concentration. From Table 1, the overall averaged comparison bias is 0.2%. Averaged value of the Pearson's moment correlations for the daily mean data at many stations is 0.75. (Comparisons using the monthly mean values show better correlations.) But several stations show noticeably discrepancy in the averaged concentration and/or in correlation coefficient. Take Tutuila, American Samoa (SMO) for example. The calculated concentration for SMO by the model agrees with the lower concentration values observed during the period 1997 to 2002. After 2003, the observed and simulated concentrations agree relatively well. There are no large, strong sources of H_2 near the SMO station and the concentration level in the free troposphere is below 600 ppb, leading to the possibility of certain local contamination. The result for the station of Tae-ahn Peninsula, Republic of Korea (TAP) shows less agreement in the statistical comparison, likely due to the effect of strong local emission.

For Cape Grim, Australia (CGO), simulated values show relatively low and the time series is characterized by spikes of low value, in disagreement with the observation. This difference is likely caused by the selective sampling procedure employed at this station in an effort to obtain "background" concentration levels. Since the sampling air is selected by using the wind direction to collect maritime air, the air mass arriving from the Australian Continent side is removed. The H_2 concentration of the air mass, which passed over the Australian Continent, will be lower than the oceanic air mass because of the strong soil uptake. When the same selection procedure is applied to the model result, the low values in the time series at CGO are removed. In Table 1, the comparison with observed and calculated value is obtained by extracting only the observed day, showing good agreement for CGO. Comparisons with other stations are discussed below.

3.2.1 Seasonal cycles

The monthly mean values of the selected 10 stations are shown in Fig. 4. The latitudinal distributions of the seasonal maximum and minimum and their timing of occurrence

are shown in Fig. 5. Previous observational and model studies have shown that the amplitudes of the seasonal cycle are large in northern high latitudes and decrease towards the tropics. The amplitudes in the southern extra-tropics are slightly higher than those in the tropics, but smaller than those of northern extra-tropics. The upper right panel of Fig. 5 shows that the model reproduces the amplitude distribution relatively well, demonstrating that the latitudinal distribution of the seasonal minimum is the major contributor to the north-south gradient.

For regions south of 30° S, the phase and amplitude of the seasonal variation are similar between the stations, with maximum and minimum occurring in austral summer and winter, respectively. Since the regional contrast of sources and sinks is small and the lifetime is longer than the timescale of transport and mixing, the H_2 concentration is well mixed. The homogeneous distribution also results in smaller synoptic variation (see the result of South Pole (SPO) in Fig. 4), expect at CGO for reasons discussed above. Novelli et al. (1999) and Hauglustaine and Ehhalt (2002) pointed out that the main influencing factor of the seasonal cycle in the Southern Hemisphere is the biomass burning. On the other hand, based on their airborne observations of H_2 and its δD ratio, Rhee et al. (2006) noted that the variation in the chemical production is a dominant factor. For CO, seasonal maximums appear during the austral spring in southern high latitudes and are highly connected to the timing of maximum biomass burning emissions in Southern Africa and Southern America. But the seasonal maximums of H_2 occur later than those of CO. In the Southern Hemisphere, the seasonal maximum and minimum of net chemical production appear in austral summer and winter, respectively, and the phasing of the H_2 seasonal cycle is linked to this rather than the variation in the biomass burning activities. We conclude that the net chemical production is the more dominant process influencing the H_2 seasonal cycle in the southern high latitudes. However, it is possible that the biomass burning can shift the timing of the occurrence of the seasonal maximum. For example, the model simulation reproduces well the shape and magnitude of the seasonal cycle at each of the stations in this region of the Southern Hemisphere, but the seasonal maximum occurs about one

month later than the observation. Since the emission magnitude from biomass burning adopted in our model is smaller than the previous model studies, the timing of seasonal maximum in our model could be caused by the lack of biomass burning emission.

The stations in the tropics and southern low latitudes such as Ascension Island, UK (ASC, in Fig. 4) and Mahe Island, Seychelles (SEY), show relatively small seasonal variation but are characterized by two peaks in spring and autumn with one large seasonal minimum between July and August. The model results capture the pattern well and suggest that the biomass burning in the northern and southern subtropics contribute to the peak in the spring and autumn, respectively. The active region of biomass burning alternates between the hemispheres around the equator in association with the timing of dry and wet season. The timing of the seasonal minimum is associated with the enhanced inflow of air from the Northern Hemisphere with low H_2 concentration, amplified by the strong soil uptake in the tropics.

The occurrence dates of the maximum and minimum are quite different between the Northern Hemisphere and the Southern Hemisphere (see Fig. 4). Around 30° N, many stations show seasonal maximums occurring between June and July. The seasonal minimums appear during the period from October to December. The seasonal variation in this region is a result of a complicated combination of source/sink change; net chemical production in the atmosphere, oceanic emission, biomass burning, and soil uptake. Variation in large-scale transport also contributes to the observed variation. In general, the model reproduces well the values of maximum and minimum at many stations, but causes both maximum and minimum to occur one to two months earlier. For inland sites near arid regions, such as Wendover, United States (UTA, in Fig. 4), Ulaan Uul, Mongolia (UUM, in Fig. 4), and Sary Taukum, Kazakhstan (KZD), large discrepancies between model and observation can be seen. Model results at these stations overestimate the concentration of the seasonal minimum near the end of the autumn. The possible cause of this is the strong uptake in the local region. In this study, the simulated deposition velocity shows large variability around the semi-arid regions, because of the high diffusivity in the soil and limited biological activity due to

water stress. It is possible that the coarseness of the model grid fails to capture the real heterogeneity of the soil types in the semi-arid regions and thus is unable to capture the strong local uptake.

For regions north of 45° N, the seasonal maximum appears in the late spring and the minimum at the beginning of the autumn at every station. The amplitude of the seasonal cycle increases poleward, reaching about 70 ppb at Alert, Canada (ALT, in Fig. 4). This latitudinal change in the amplitude is related to the poleward decrease in the value of the seasonal minimum. The model results agree well in the timing of the occurrence of the seasonal maximum/minimum, as well as in the maximum value, but slightly underestimate the seasonal minimum. This problem is connected with the representation of the physical property of the uppermost soil. There still is a great deal of uncertainty associated with the air ratio at the soil surface, which is influenced by the melting of frozen soil in their summer. In addition, it is conceivable that the biologically inactive layer is thinner in this region. The soil temperature in this region remains relatively low even in the summer and this can decrease the thickness of the inactive layer. At stations along the Pacific rim, such as Shemya Island, United States (SHM, in Fig. 4) and Cold Bay, United States (CBA), the concentrations decrease with large day-to-day variation from summer to autumn. These variations are related to the variation in the transport of maritime and continental air masses with different H_2 concentration caused by enhanced summer emission of H_2 by the ocean and by strong soil uptake on the continent.

3.2.2 Global distribution, budgets and trend of H_2

The global distributions of simulated H_2 concentration at the surface and 250 hPa in January, April, July, and October are shown in Fig. 6. Zonal averages of H_2 distribution for the same months are shown in Fig. 7. The horizontal and vertical distributions of H_2 concentration are relatively uniform south of 45° S, caused by the absence of strong surface sources and sinks. In southern mid latitudes, H_2 concentration in the free troposphere shows a zonal average of 530–540 ppb year-round. The concentration

Full Screen / Esc

Printer-friendly Version

Interactive Discussion

near the ocean surface during the austral summer at this latitudinal band is 5–10 ppb higher than in the upper troposphere, due mainly to the presence of oceanic sources. In contrast, the concentration over the land surface indicates values 10–30 ppb lower than those in the free troposphere due to the soil uptake. In the tropical region, the oceanic emission and net chemical production of H_2 are relatively high throughout the year. In addition, biomass burning emits large amounts of H_2, especially during boreal spring and autumn, at least partially offsetting the large soil uptake.

The tropics and subtropics are regions where emissions of biogenic NMVOCs are strong and cumulus convection is active. This results in a strong vertical transport to the upper troposphere of NMVOCs and NO_x from both the biogenic and pyrogenic sources at the surface. Enhanced chemical reactions result in a higher production of H_2 at the 200–300 hPa levels, compared to the situation in the lower free troposphere. However, vertical transport of low-H_2 air mass affected by the soil uptake results in a region of relatively low H_2 concentration in the uppermost troposphere of the subtropics, mainly over the continents.

The Northern Hemisphere shows large seasonally varying vertical gradients in H_2, with the maximum occurring in boreal spring and autumn, respectively. The lowest concentration is seen near the surface of northern high latitudes, with low concentration areas spreading to the upper troposphere and lower latitudes. The contrast in the concentration between land and ocean is large in northern mid- and high-latitudes. Anthropogenic emissions are strong in areas with large population, such as North America, Europe, and China, resulting in high H_2 concentrations, especially over the China and India. In the summer (July, Fig. 6c), we see an area of high H_2 concentration over East Asia and Southeast Asia spreading to the western Pacific and farther east along the subtropical Pacific with slightly lower concentration, indicating an enhanced transport of oceanic air mass associated with the Asian monsoon.

The global H_2 budget obtained by our model is summarized in Table 2, along with the results published in previous studies. The annual global averages of the simulated chemical source and sink for the period 1997 to 2005 are in the range of 36–

37 Tg yr^{-1} and 17–18 Tg yr^{-1}, with respective average values of 36.6 ± 0.3 Tg yr^{-1} and 18.1 ± 0.2 Tg yr^{-1}. The annual total flux of soil uptake has a range of 54–57 Tg yr^{-1}, with an average value of 56.2 ± 0.9 Tg yr^{-1}. These values correspond relatively well with values obtained by other forward models (Hauglestain and Ehhalt, 2002; Sander-
5 son et al., 2003; Price et al., 2007). However, Rhee et al. (2006) and Xiao et al. (2007) reported a larger estimate of soil uptake flux (88 and 85 Tg yr^{-1}, respectively) and chemical production (64 and 77 Tg yr^{-1}, respectively). The larger production values resulted from the assumption of larger production from the oxidation of NMVOCs. Ehhalt and Rohrer (2009) pointed out that the estimate of the soil uptake has large uncer-
10 tainty, and advocated 55 +30/−20 Tg yr^{-1}, which brings it closer to our results. The estimate by Rhee et al. (2006) was based on a simplified calculation involving the seasonal variation of the concentration and isotope ratio of H$_2$ in the free northern mid-latitude troposphere. They assumed that the Northern Hemisphere troposphere is well mixed and that soil uptake and net chemical production contribute uniformly in vertical.
15 However, as noted above, the footprint of the soil uptake in the upper troposphere is mediated by the vertical convective transport in the tropics and subtropics, resulting in temporal and spatial heterogeneity in the H$_2$ concentration. Furthermore, a global simulation of H$_2$ isotope by Price et al. (2007) showed that the ground observations of δD could be explained by a smaller H$_2$ soil uptake than that estimated by Rhee et
20 al. (2006). Xiao et al. (2007), on the other hand, used an inversion method with a 2-D multi-box model employing relatively few observations to constrain their results. One of the problems with this approach is that the seasonal variation of H$_2$ near the surface is quite different over the ocean and land, causing the 2-D inversion to be sensitive to the station location. When many observation points near the continent are used, the
25 influence of soil uptake may be overestimated. In our model, the soil uptake is calculated online and agrees with the uptake value endorsed by Ehhalt and Rohrer (2009). Furthermore, NMVOCs are calculated online each time step, and their emissions are optimized to reproduce the observed CO and NMVOCs concentrations.

Novelli et al. (1999) showed that tropospheric H_2 does not display a clear increasing or decreasing trend after 1995, in agreement with our results shown in Fig. 3. Globally averaged source/sink H_2 anomalies and the corresponding tropospheric burden are shown in Fig. 8. Superimposed on the gradual total emission increase due mainly to growing anthropogenic emissions, there is a noticeable inter-annual variability caused by emissions from large biomass burnings. Especially the emission from the Indonesian fires during 1997–1998, and from the forest fires in Siberia in 1998 are significant. In contrast, year 2000 saw very little biomass burning. We also see inter-annual variability in the soil uptake flux of H_2, offsetting the emissions. The net total emission from the surface, along with the chemical production, of H_2 is reflected in the tropospheric burden of H_2, which shows a slight increasing (but not significant) trend from 2002 to 2005. The biomass burning in 1998 brought a temporary increase in the tropospheric burden but recovered in about two years. The observed H_2 concentration also shows a corresponding peak during 1997–1998 (Fig. 3). The summertime increase in 1998 was observed at nearly all stations and the model is found to reproduce it relatively well. Both the chemical production and loss show an increasing trend. It is possible that this increase is related to an increase in the methane oxidation rate caused by an increase in global temperature, and/or is related to an increase in OH radical caused by an increase in the water vapor. However, the amount of change is very small compared to changes in the surface emission.

The soil uptake not only responds to an increase in atmospheric concentration but also to changes in soil temperature and moisture. The long-term variations in the total and average values of simulated soil uptake flux, deposition velocity, and soil moisture in four latitude bands are shown in Fig. 9. They are obtained by applying the curve fitting method of Nakazawa et al. (1997). From the figure, both the soil uptake flux and the deposition velocity in the tropics show noticeable inter-annual variation compared to other latitudinal bands. In 2000, we see a decrease in the deposition velocity correlated with an increase in soil moisture caused by increase in precipitation over land. By examining the normalized Southern Oscillation index (SOI) obtained by

Ropelewski and Halpert (1987) (also shown in Fig. 9), the increase in soil moisture in 2000 is linked to an increase in precipitation around Indonesia caused by a La Nina event. Although an increase in precipitation on land in a tropical region decreases the soil uptake of H_2, it actually reduces the frequency of biomass burning in the same area. This balance between the reduced emission and reduced soil uptake results in very little change in atmospheric H_2, as was the case in the tropics in 2000 (Fig. 2).

3.3 Possible uncertainty of soil uptake flux

In the soil diffusion model used in this study, the factors that produce uncertainties in the soil estimate are the diffusion coefficient in soil, the degree of biological activity, and the inactive layer thickness. The diffusivity and the biological activity are determined by the air ratio in the soil, soil moisture, and soil temperature. Prediction errors of these variables are expected to affect the deposition velocity of H_2. The good agreement between our model result and the observations gives indirect support to the ability of our model to reproduce relatively well the soil moisture and temperature in general. Furthermore, inter-annual variations in the soil variables do not appear to produce large variations in the global soil uptake, thus having minimal impact on the budget of tropospheric H_2. The factor that produces greater uncertainty is associated with the specification of soil properties, such as the ratio of soil surface area to the aerial volume, and the ratio of the volume of solids. The change in the physical structure of the soil within the first several centimeters from the surface is large. This demands a better and more detailed distribution of soil variables with fine vertical resolution in the top soil layer. In this study, the correction of $\sim 0.2\,\mathrm{g\,g^{-1}}$ is uniformly applied to the air ratio in consideration of vertical ununiformity of the air ratio at the uppermost layer. However, this correction is not enough to capture a sharp change of the air ratio near the surface.

The reproducibility of the observations from the stations near semi-arid regions in central Asia and North America is not good in this study. The seasonal minimum of H_2 concentration cannot be reproduced well, probably caused by an underestimation of

the deposition velocity around the observation stations. Semi-arid regions have a large potential for H_2 uptake but this uptake is prevented by the dryness. That is, the soil uptake of H_2 in a semi-arid region is highly sensitive to change in the vertical distribution of soil moisture. A better representation of arable fields is also important in improving the estimation of global H_2 uptake by the soil. Although we do not carry out model verification in regards to the H_2 uptake by the arable land, we realize that seasonal changes in the surface condition and in the vertical soil properties are significant and will likely have a large impact on the soil uptake estimate. Large variations in soil properties and the inactive layer thickness caused by strong sunlight can take place over a short time period.

The global distribution of the inactive layer thickness is practically not known. The formation of the inactive layer is mainly due to the irreversible destruction of enzymes or bacteria near the surface soil. Thus, the temporal change in the inactive layer thickness is influenced not only by the physical stress such as extreme heating and drying but also by the recovery/redistribution rate of microbes and enzymes. Figure 10 shows the sensitivity of the annually averaged deposition velocity on land to the thickness of the inactive layer δ. The figure shows a near 50% difference in the deposition velocity between $\delta = 0$ and $\delta = 1.0$ cm. This is equivalent to 25–30 Tg yr^{-1} difference in global soil uptake, which is not negligible, considering the size of the global H_2 budget. In this study, $\delta = 0.7$ cm was adopted, because it optimizes the agreement with the observation. With the assumption that δ has a range of 0.3 to 1.4 cm, we obtain an uncertainty of $\pm 20\%$ for the estimated deposition velocity over the land which gives ± 12 Tg yr^{-1} uncertainty for a global soil uptake estimate. Although the assumed range of δ is consistent with those estimated by other investigators (Yonemura et al., 2000b; Shmitt et al., 2009), we need much more observations to obtain a more realistic idea of the horizontal distribution and the seasonal variation of the inactive layer.

4 Conclusions

We have conducted a global simulation of tropospheric H_2 concentrations and evaluated its uptake by land using the global chemical transport model, CHASER. The soil diffusion model, which has an inactive and active layer of biological consumption rate, is incorporated into the dry deposition scheme. The variation in the soil diffusivity and biological activity in the soil are calculated as a function of soil temperature and moisture, which are calculated as prognostic variables in the land process module of the model. The model results of the regional distribution and seasonal variation of the H_2 deposition velocity agree relatively well with the observed values obtained by other investigators.

A large seasonal variation in the deposition velocity corresponding to changes in soil temperature and snowfall is seen in the northern high latitudes. In the mid-latitudes of both hemispheres and the tropics, we can identify two regional types where (1) biogenic uptake is active because of the warm climate, but the wet environment counters diffusion to the soil, and (2) biological activity becomes weaker due to high temperature and dryness, but the dry climate makes the transportation in the soil more efficient. The strength of soil uptake is closely related to the water and heat budget in each region.

The H_2 concentration calculated by the model reproduces relatively well the concentration observed at the NOAA stations. The seasonal variation of the concentration in the Southern Hemisphere is mainly due to the net chemical production in austral summer and the inflow of the relatively low H_2 air mass from the north following the north-south transport in austral winter. The vertical and horizontal gradients are small in the Southern Hemisphere. In the tropics, both the net chemical production and the soil uptake are high through the year and the impact of biomass burning is superimposed during January and September. Furthermore, in the tropical region, active cumulus convection transports air mass influenced by both the soil uptake and biomass burning near the surface to the upper troposphere. Biogenic NMVOCs are also transported to high altitudes over the Amazon and Africa, allowing for frequent production of H_2 by chemical reactions. Seasonal variation in the soil uptake is a dominant contributor

to the H_2 variation in the Northern Hemisphere. During the boreal summer, a strong uptake by the soil surface produces a large vertical gradient, land-sea gradient, and latitudinal gradient in the H_2 concentration.

For our simulation period of 1997 to 2005, the average tropospheric burden and lifetime are found to be 150 Tg and 2.0 year, respectively. The annual total amount of chemical production, chemical loss, and soil uptake are 36, 18, 56 Tg yr^{-1}, respectively. The budget calculated from our simulation agrees with the lower end of the estimated values obtained by previous forward model studies.

Our model is able to reproduce the overall inter-annual variation observed during the period 1997–2005. Large H_2 concentration peaks caused by large biomass burning in Indonesia and Siberia were observed in 1997 and 1998, respectively at nearly all stations. Our model is able to successfully reproduce these peaks.

Although the anthropogenic emission has been increasing over the last several years, the tropospheric H_2 concentration shows no significant long-term trend. Our model result shows that the soil uptake flux changes in the direction that offsets the increase in H_2 emission to the atmosphere. The simulated H_2 deposition velocity shows a small trend and inter-annual variation. We conclude that the recent decadal climate change has had very little impact on the H_2 concentration.

The global soil uptake flux of H_2 obtained by our model succeeds in reproducing the tropospheric H_2 concentration and its seasonal variation observed at many of the stations distributed throughout the world. However, in regions where one has a strong H_2 uptake, uncertainties in both uptake flux and atmospheric concentration are still large. In order to improve the estimate of the soil uptake flux and to reproduce/predict the present/future concentration of H_2 in the atmosphere, it is necessary to develop a detailed knowledge of the vertical structure of physical soil properties and the response behavior of the microbial activity in the shallow top layer of the soil. In particular, significant improvement in the understanding and reproducibility of soil properties of the arable land and the semi-arid region, where soil temperature and moisture can change drastically over a short time period, is required.

Full Screen / Esc

Printer-friendly Version

Interactive Discussion

References

Andreae, M. O. and Merlet, P.: Emission of trace gases and aerosols from biomass burning, Global Biogeochem. Cy., 15, 955–966, 2001.

Atkinson, R., Baulch, D. L., Cox, R. A., Crowley, J. N., Hampson, R. F., Hynes, R. G., Jenkin, M. E., Rossi, M. J., and Troe, J.: Evaluated kinetic and photochemical data for atmospheric chemistry: Volume I – gas phase reactions of O_x, HO_x, NO_x and SO_x species, Atmos. Chem. Phys., 4, 1461–1738, doi:10.5194/acp-4-1461-2004, 2004.

Conrad, R.: Soil microorganisms as controllers of atmospheric trace gases (H_2, CO, CH_4, OCS, N_2O, and NO), Microbiol. Rev., 60, 609–640, 1996.

Conrad, R. and Seiler, W.: Influence of temperature, moisture, and organic carbon on the flux of H_2 and CO between soil and atmosphere: field studies in subtropical regions, J. Geophys. Res., 90, 5699–5709, 1985.

Conrad, R., Weber, M., and Seiler, W.: Kinetics and electron transport of soil hydrogenases catalyzing the oxidation of atmospheric hydrogen, Soil Biol. Biochem., 15(2), 167–173, doi:10.1016/0038-0717(83)90098-6, 1983.

Constant, P., Chowdhury, S. P., Pratscher, J., and Conrad, R.: Streptomycetes contributing to atmospheric molecular hydrogen soil uptake are widespread and encode a putative high-affinity [NiFe]-hydrogenase, Environmental Microbiology, 12, 821–829, doi:10.1111/j.1462-2920.2009.02130.x, 2010.

Ehhalt, D. H. and Rohrer, F.: The tropospheric cycle of H_2: a critical review, Tellus B, 61, 500–535, doi:10.1111/j.1600-0889.2009.00416.x, 2009.

Guenther, A., Hewitt, C. N., Erickson, D., Fall, R., Geron, C., Graedel, T., Harley, P., Klinger, L., Lerdau, M., Mckay, W. A., Pierce, T., Scholes, B., Steinbrecher, R., Raja, T., Taylor, J., and

Zimmerman, P.: A global model of natural volatile organic compound emissions, J. Geophys. Res., 100, 8873–8892, 1995.

Hauglustaine, D. A. and Ehhalt, D. H.: A three-dimensional model of molecular hydrogen in the troposphere, J. Geophys. Res., 107, 4330, doi:10.1029/2001JD001156, 2002.

Hirabayashi, Y., Kanae, S., Struthers, I., and Oki, T.: A 100-year (1901–2000) global retrospective estimation of the terrestrial water cycle, J. Geophys. Res., 110, D19101, doi:10.1029/2004JD005492, 2005.

K-1 Model Developers,: K-1 coupled model (MIROC) description, in: K-1 technical report, edited by: Hasumi, H. and Emori, S., 34 pp., available at: the Center for Climate System Research, University of Tokyo, http://www.ccsr.u-tokyo.ac.jp/~agcmadm/], 2004.

Koster, R. D., Dirmeyer, P. A., Guo, Z. C., Bonan, G., Chan, E., Cox, P., Gordon, C. T., Kanae, S., Kowalczyk, E., Lawrence, D., Liu, P., Lu, C. H., Malyshev, S., McAvaney, B., Mitchell, K., Mocko, D., Oki, T., Oleson, K., Pitman, A., Sud, Y. C., Taylor, C. M., Verseghy, D., Vasic, R., Xue, Y. K., and Yamada, T.: Regions of strong coupling between soil moisture and precipitation, Science, 305, 1138–1140, 2004.

Lallo, M., Aalto, T., Laurila, T., and Hatakka, J.: Seasonal variations in hydrogen deposition to boreal forest soil in southern Finland,:= Geophys. Res. Lett., 35, L04402, doi:10.1029/2007GL032357, 2008.

Millington, R. J. and Quirk, J. P.: Permeability of porous media, Nature, 183, 387–388, 1959.

Miyazaki, K., Iwasaki, T., Shibata, K., Deushi, M., and Sekiyama, T.: The impact of changing meteorological variables to be assimilated into GCM on ozone simulation with MRI CTM, J. Meteor. Soc. Japan, 83, 909–918, 2005.

Müller, J.-F.: Geographical distribution and seasonal variation of surface emissions and deposition velocities of atmospheric trace gases, J. Geophys. Res., 97, 3787–3804, 1992.

Novelli, P. C., Lang, P. M., Masarie, K. A., Hurst, D. F., Myers, R., and Elkins, J. W.: Molecular hydrogen in the troposphere: global distribution and budget, J. Geophys. Res., 104, 30427–30444, 1999.

Ohara, T., Akimoto, H., Kurokawa, J., Horii, N., Yamaji, K., Yan, X., and Hayasaka, T.: An Asian emission inventory of anthropogenic emission sources for the period 1980–2020, Atmos. Chem. Phys., 7, 4419–4444, doi:10.5194/acp-7-4419-2007, 2007.

Olivier, J. G. J., Van Aardenne, J. A., Dentener, F., Ganzeveld, L., and Peters, J. A. H. W.: Recent trends in global greenhouse gas emissions: regional trends and spatial distribution of key sources, in: Non-CO2 Greenhouse Gases (NCGG-4), edited by: van Amstel, A.,

325–330, Millpress, Rotterdam, 2005.

Onogi, K., Tsutsui, J., Koide, H., Sakamoto, M., Kobayashi, S., Hatsushika, H., Matsumoto, T., Yamazaki, N., Kamahori, H., Takahashi, K., Kadokura, S., Kato, K., Oyama, R., Ose, T., Mannoji, N., and Taira, R.: The JRA-25 Reanalysis, J. Meteor. Soc. Japan, 85, 369–432, 2007.

Prather, M. J.: An environmental experiment with H2?, Science, 302, 581–582, 2003.

Price, H., Jaegle, L., Rice, A., Quay, P., Novelli, P. C., and Gammon, R.: Global budget of molecular hydrogen and its deuterium content: constraints from ground station, cruise, and aircraft observations, J. Geophys Res., 112, D22108, doi:10.1029/2006JD008152, 2007.

Rhee, T. S., Brenninkmeijer, C. A. M., and Röckmann, T.: The overwhelming role of soils in the global atmospheric hydrogen cycle, Atmos. Chem. Phys., 6, 1611–1625, doi:10.5194/acp-6-1611-2006, 2006.

Ropelewski, C. F. and Halpert, M. S.: Global and regional scale precipitation patterns associated with the El Nino/Southern Oscillation, Mon. Weather Rev., 115, 1606–1626, 1987.

Sanderson, M. G., Collins, W. J., Derwent, R. G., and Johnson, C. E.: Simulation of global hydrogen levels using a Lagrangian three-dimensional model, J. Atmos. Chem., 46, 15–28, 2003.

Schmidt, M., Hanselmann, U., Wollschlager, U., Hammer, S., and Levin, I.: Investigation of parameters controlling the soil sink of atmospheric molecular hydrogen, Tellus B, 61, 416–423, 2008.

Schultz, M. G., Diehl, T., Brasseur, G. P., and Zittel, W.: Air pollution and climate-forcing impacts of a global hydrogen economy, Science, 302, 624–627, 2003.

Sekiguchi, M. and Nakajima, T.: A k-distribution-based radiation code and its computational optimization for an atmospheric general circulation model, J. Quant. Spectrosc. Ra., 109, 2779–2793, 2008.

Shindell, D., Faluvegi, G., Stevenson, D., Krol, M., Emmons, L., Lamarque, J.-F., Petron, G., Dentener, F., Ellingsen, K., Schultz, M., Wild, O., Amann, M., Atherton, C., Bergmann, D., Bey, I., Butler, T., Cofala, J., Collins, W., Derwent, R., Doherty, R., Drevet, J., Eskes, H., Fiore, A., Gauss, M., Hauglustaine, D., Horowitz, L., Isaksen, I., Lawrence, M., Montanaro, V., Muller, J.-F., Pitari, G., Prather, M., Pyle, J., Rast, S., Rodriguez, J., Sanderson, M., Savage, N., Strahan, S., Sudo, K., Szopa, S., Unger, N., van Noije, T., and Zeng, G.: Multimodel simulations of carbon monoxide: Comparison with observations and projected near-future changes, J. Geophys. Res., 111, D19306, doi:10.1029/2006JD007100, 2006.

Smith-Downey, N. V.: Soil uptake of molecular hydrogen and remote sensing of soil freeze and thaw, Ph.D. thesis, 116 pp., Calif. Inst. of Technol., Pasadena, CA, 2006.

Smith-Downey, N. V., Randerson, J. T., and Eiler, J. M.: Temperature and moisture dependence of soil H_2 uptake measured in the laboratory, Geophys. Res. Lett., 33, L14813, doi:10.1029/2006GL026749, 2006.

Smith-Downey, N. V., Randerson, J. T., and Eiler, J. M.: Molecular hydrogen uptake by soil in forest, desert and marsh ecosystems in California, J. Geophys. Res., 113, G03037, doi:10.1029/2008JG000701, 2008.

Sudo, K. and Akimoto, H.: Global source attribution of tropospheric ozone: Long-range transport from various source regions, J. Geophys. Res., 112, D12302, doi:10.1029/2006JD007992, 2007.

Sudo, K., Takahashi, M., Kurokawa, J., and Akimoto, H.: CHASER: A global chemical model of the troposphere: 1. Model description, J. Geophys. Res., 107(D17), 4339, doi:10.1029/2001JD001113, 2002a.

Sudo, K., Takahashi, M., and Akimoto H.: CHASER: A global chemical model of the troposphere: 2. Model results and evaluation, J. Geophys. Res., 107(D21), 4586, doi:10.1029/2001JD001114, 2002b.

Takata, K., Emori, S., and Watanabe, T.: Development of the Minimal Advanced Treatments of Surface Interaction and RunOff (MATSIRO), Global Planet. Change, 38, 209–222, 2003.

Tromp, T. K., Shia, R.-L., Allen, M., Eiler, J. M., and Yung, Y. L.: Potential environmental impact of a hydrogen economy on the stratosphere, Science, 300, 1740–1742, 2003.

Warwick, N. J., Bekki, S., Nisbet, E. G., and Pyle, J. A.: Impact of a hydrogen economy on the stratosphere and tropo- sphere studied in a 2-D model, Geophys. Res. Lett., 31, L05107, doi:10.1029/2003GL019224, 2004.

Watanabe, S., Miura, H., Sekiguchi, M., Nagashima, T., Sudo, K., Emori, S., and Kawamiya, M.: Development of an atmospheric general circulation model for integrated Earth system modeling on the Earth simulator, J. Earth Simulator, 9, 28–35, 2008.

van der Werf, G. R., Randerson, J. T., Giglio, L., Collatz, G. J., Kasibhatla, P. S., and Arellano Jr., A. F.: Interannual variability in global biomass burning emissions from 1997 to 2004, Atmos. Chem. Phys., 6, 3423–3441, doi:10.5194/acp-6-3423-2006, 2006.

van Noije, T. P. C., Eskes, H. J., Dentener, F. J., Stevenson, D. S., Ellingsen, K., Schultz, M. G., Wild, O., Amann, M., Atherton, C. S., Bergmann, D. J., Bey, I., Boersma, K. F., Butler, T., Cofala, J., Drevet, J., Fiore, A. M., Gauss, M., Hauglustaine, D. A., Horowitz, L. W., Isaksen,

Chemical transport model simulation

H. Yashiro et al.

I. S. A., Krol, M. C., Lamarque, J.-F., Lawrence, M. G., Martin, R. V., Montanaro, V., Müller, J.-F., Pitari, G., Prather, M. J., Pyle, J. A., Richter, A., Rodriguez, J. M., Savage, N. H., Strahan, S. E., Sudo, K., Szopa, S., and van Roozendael, M.: Multi-model ensemble simulations of tropospheric NO2 compared with GOME retrievals for the year 2000, Atmos. Chem. Phys., 6, 2943–2979, doi:10.5194/acp-6-2943-2006, 2006.

Wesely, M. L.: Parameterization of surface resistances to gaseous dry deposition in regional-scale numerical models, Atmos. Environ., 23, 1293–1304, 1989.

Xiao, X., Prinn, R. G., Simmonds, P. G., Steele, L. P., Novelli, P. C., Huang, J., Langenfelds, R. L., O'Doherty, S., Krummel, P. B., Fraser, P. J., Porter, L. W., Weiss, R. F., Salameh, P., and Wang, R. H. J.: Optimal estimation of the soil uptake of molecular hydrogen from the Advanced Global Atmospheric Gases Experiments and other measurements, J. Geophys. Res., 112, D07303, doi:10.1029/2006JD007241, 2007.

Yonemura, S., Kawashima, S., and Tsuruta, H.: Continuous measurements of CO and H_2 deposition velocities onto an andisol: uptake control by soil moisture, Tellus 51B, 688–700, 1999.

Yonemura, S., Yokozawa, M., Kawashima, S., and Tsuruta, H.: Model analysis of the influence of gas diffusivity in soil on CO and H_2 uptake, Tellus, 52B, 919–933, 2000a.

Yonemura, S., Kawashima, S., and Tsuruta, H.: Carbon monoxide, hydrogen, and methane uptake by soils in a temperate arable field and a forest, J. Geophys. Res., 105, 14347–14362, 2000b.

Title Page

Abstract | Introduction

Conclusions | References

Tables | Figures

◄ | ►

◄ | ►

Back | Close

Full Screen / Esc

Printer-friendly Version

Interactive Discussion

Table 1. Averaged concentrations, amplitude of seasonal cycles, and Pearson's moment correlations between observed and simulated value for all sites considered in this study. Bias is calculated by (Model-Obs.)/Obs. and Ratio is obtained by Model/Obs.

| | SITE | | | | Mean Conc. | | | Amplitude of Season. Cycle | | | |
| | | | | Datapoints for | | | | | | | |
abbr	Name (Latitude , Longitude, Elevation)	Period	comparison	Obs.	Model	Bias [%]	Obs.	Model	Ratio [%]	Corr. Coef.
ALT	*Alert (82.5° N, 62.5° W, 210 m)*	1997/01–2005/06	1328	488.2	495.1	1.4	71.6	59.5	83	0.84
ASC	*Ascension Island (7.9° S, 14.4° W, 54 m)*	1997/01–2005/06	1467	540.3	541.1	0.1	14.9	7.4	50	0.38
ASK	*Assekrem (23.3° N, 5.6° E, 2710 m)*	1997/01–2005/06	600	541.2	523.4	−3.3	21.1	25.2	120	0.31
AZR	*Terceira Island (38.8° N, 27.4° W, 40 m)*	1997/01–2005/05	630	510.6	516.1	1.1	30.5	38.4	126	0.60
BAL	*Baltic Sea (55.4° N, 17.2° E, 28 m)*	1997/01–2005/06	1456	510.7	499.6	−2.2	39.6	43.6	110	0.68
BME	*St. David's Head (32.4° N, 64.7° W, 30 m)*	1997/01–2005/06	657	523.6	519.8	−0.7	38.3	40.7	106	0.62
BMW	*Tudor Hill (32.3° N, 64.9° W, 30 m)*	1997/01–2005/06	632	527.6	521.6	−1.1	39.6	41.0	104	0.60
BRW	*Barrow (71.3° N, 156.6° W, 11 m)*	1997/01–2005/07	1815	493.5	493.9	0.1	61.9	60.6	98	0.81
BSC	*Black Sea (44.2° N, 28.7° E, 3 m)*	1997/01–2005/06	803	525.7	494.1	−6.0	53.9	38.7	72	0.36
CBA	*Cold Bay (55.2° N, 162.7° W, 25 m)*	1997/01–2005/07	1639	499.5	503.8	0.9	51.2	59.7	116	0.79
CGO	*Cape Grim (40.7° S, 144.7° E, 94 m)*	1997/01–2005/06	806	536.7	539.8	0.6	21.7	17.9	82	0.68
CHR	*Christmas Island (1.7° N, 157.2° W, 3 m)*	1997/01–2005/06	537	544.3	543.2	−0.2	12.7	11.3	90	0.26
CRZ	*Crozet (46.5° S, 51.9° E, 120 m)*	1997/01–2005/06	523	535.8	540.4	0.9	17.4	17.2	99	0.42
EIC	*Easter Island (27.1° S, 109.5° W, 50 m)*	1997/01–2005/06	565	541.7	540.5	−0.2	19.8	13.0	66	0.41
GMI	*Guam (13.4° N, 144.8° E, 2 m)*	1997/01–2005/06	1538	538.6	541.2	0.5	20.5	21.6	105	0.59
HBA	*Halley Bay (75.6° S, 26.5° W, 33 m)*	1997/01–2005/06	818	538.0	539.5	0.3	20.9	18.1	87	0.53
HUN	*Hegyhatsal (47.0° N, 16.7° E, 248 m)*	1997/01–2005/06	793	520.3	505.3	−2.9	41.5	36.6	88	0.67
ICE	*Heimaey (63.4° N, 20.3° W, 100 m)*	1997/01–2005/06	728	500.3	494.3	−1.2	49.4	50.8	103	0.77
ITN	*Grifton (35.4° N, 77.4° W, 505 m)*	1997/01–1999/06	262	530.4	521.0	−1.8	50.1	41.8	84	0.73
IZO	*Tenerife (28.3° N, 16.5° W, 2360 m)*	1997/01–2005/06	669	531.4	523.0	−1.6	25.6	25.4	99	0.52
KEY	*Key Biscayne (25.7° N, 80.2° W, 3 m)*	1997/01–2005/06	655	545.6	532.1	−2.5	36.1	33.7	93	0.35
KUM	*Cape Kumukahi (19.5° N, 154.8° W, 3 m)*	1997/01–2005/06	1734	511.4	529.6	3.6	28.9	29.7	103	0.66
KZD	*Sary Taukum (44.5° N, 75.6° E, 412 m)*	1997/10–2005/06	701	452.6	488.3	7.9	103.1	35.1	34	0.48
KZM	*Plateau Assy (43.3° N, 77.9° E, 2519 m)*	1997/10–2005/06	707	498.4	510.2	2.4	19.2	31.9	166	0.23
LEF	*Park Falls (45.9° N, 90.3° W, 868 m)*	1997/01–2005/06	872	494.9	496.3	0.3	57.7	46.3	80	0.75
MHD	*Mace Head (53.3° N, 9.9° W, 25 m)*	1997/01–2005/06	754	512.5	509.0	−0.7	44.0	46.4	106	0.83
MID	*Sand Island (28.2° N, 177.4° W, 8 m)*	1997/01–2005/06	801	526.6	527.3	0.1	34.6	33.8	98	0.78
MLO	*Mauna Loa (19.5° N, 155.6° W, 3397 m)*	1997/01–2005/06	1666	531.9	533.3	0.3	20.7	20.8	101	0.49
NWR	*Niwot Ridge (40.1° N, 105.6° W, 3523 m)*	1997/01–2005/06	849	516.0	524.9	1.7	25.9	18.7	72	0.54
PSA	*Palmer Station (64.9° S, 64.0° W, 10 m)*	1997/01–2005/06	798	536.4	539.9	0.7	23.2	18.5	80	0.69
RPB	*Ragged Point (13.2° N, 59.4° W, 45 m)*	1997/01–2005/06	778	538.9	530.5	−1.6	20.2	19.5	97	0.56
SEY	*Mahe Island (4.7° S, 55.2° E, 7 m)*	1997/01–2005/06	747	544.0	544.3	0.1	21.7	10.1	46	0.47
SHM	*Shemya Island (52.7° N, 174.1° E, 40 m)*	1997/01–2005/06	810	500.9	503.2	0.5	51.8	60.6	117	0.87
SMO	*Tutuila (14.2° S, 170.6° W, 42 m)*	1997/01–2005/06	1434	556.1	543.8	−2.2	17.1	8.8	52	0.01
SPO	*South Pole (90.0° S, 24.8° W, 2810 m)*	1997/01–2005/06	1332	535.5	535.9	0.1	18.9	16.7	88	0.46
STM	*Ocean Station "M" (66.0° N, 2.0° E, 5 m)*	1997/01–2005/07	1577	506.5	501.4	−1.0	43.2	50.3	116	0.83
SYO	*Syowa Station (69.0° S, 39.6° E, 21 m)*	1997/01–2005/06	392	538.2	539.4	0.2	21.8	17.6	81	0.56
TAP	*Tae-ahn Peninsula (36.7° N, 126.1° E, 20 m)*	1997/01–2005/06	801	529.3	548.0	3.5	76.2	51.1	67	0.59
TDF	*Tierra del Fuego (54.9° S, 68.5° W, 20 m)*	1997/05–2005/05	219	535.9	537.7	0.3	22.6	17.3	76	0.77
UTA	*Wendover (39.9° N, 113.7° W, 1320 m)*	1997/01–2005/06	792	492.4	518.0	5.2	77.4	26.9	35	0.44
UUM	*Ulaan Uul (44.5° N, 111.1° E, 914 m)*	1997/01–2005/06	824	476.4	492.8	3.4	66.0	44.0	67	0.51
WIS	*Sede Boker (31.1° N, 34.9° E, 400 m)*	1997/01–2005/06	860	521.5	515.7	−1.1	35.7	27.7	78	0.57
WLG	*Mt. Waliguan (36.3° N, 100.9° E, 3810 m)*	1997/01–2005/07	577	504.6	518.7	2.8	23.7	28.8	122	0.48
ZEP	*Zeppelinfjellet (78.9° N, 11.9° E, 475 m)*	1997/01–2005/06	1005	496.7	498.3	0.3	50.5	55.7	110	0.80
	Total	1997/01–2005/06	40043	518.5	519.6	0.2				0.75

Discussion Paper | Discussion Paper | Discussion Paper | Discussion Paper

ACPD

11, 4059–4103, 2011

Chemical transport model simulation

H. Yashiro et al.

| Title Page |
Abstract	Introduction
Conclusions	References
Tables	Figures
I◄	►I
◄	►
Back	Close
Full Screen / Esc
Printer-friendly Version
Interactive Discussion

Table 2. Global tropospheric sources and sinks of H_2 (TgH_2 yr^{-1}).

	Novelli et al. (1999)	Hauglustain and Ehhalt (2002)	Sanderson et al. (2003)	Rhee et al. (2006)	Price et al. (2007)	Xiao et al. (2007)	Ehhalt and Rohrer (2009)	This Study[a]
Anthropogenic (FF+BF)	15±10	16	20.0	15±6	23.7	15±10	11±4	15.1–15.4
Fossil fuel, industrial(FF)			(18.3)					
Biofuel(BF)				(4.4)				
Biomass Burning	16±5	13	20.0	16±3	10.1	13±3	15±6	8–15
Biogenic N2 fixation Ocean	3±2	5	4.0	6±5	6.0		6±3	6
Land	3±1	5	4.0	6±5			3±2	3
Total surface source	37	39	48	43	39.8	28	35	30–37
Total chemical reaction source	40	31	30.2	64±12	34.3	77±10	41±11	36–37
Total source	77±16	70	78.2	107±15	73	105±10	76±14	69–76
Soil uptake	56±41	55	58.3	88±11	55±8.3	85±5	60^{+30}_{-20}	54–57±12[b]
Total chemical reaction sink	19±5	15	17.1	19±3	18	18±3	19±5	17–18
Total Sink	75±41	70	75.4	107±11	73	107±11	79^{+30}_{-20}	73–76
burden	155±10	136	172	150	141	149±23	155±10	150
tropospheric lifetime	2.1	1.9	2.3	1.4	1.9	1.4	2	2

[a] The range given represents the range of annual average for model simulation time period (1997–2005).

[b] The uncertainty estimated in this study (see Sect. 3.3).

Fig. 1. Monthly mean distribution of simulated deposition velocity **(a, b)**, diffusivity in the soil **(c, d)**, uptake rate of biological H$_2$-consumption **(e, f)** for January and July. The values are averaged over the period 1997–2005.

Title Page

Abstract | Introduction

Conclusions | References

Tables | Figures

◀ | ▶

◀ | ▶

Back | Close

Full Screen / Esc

Printer-friendly Version

Interactive Discussion
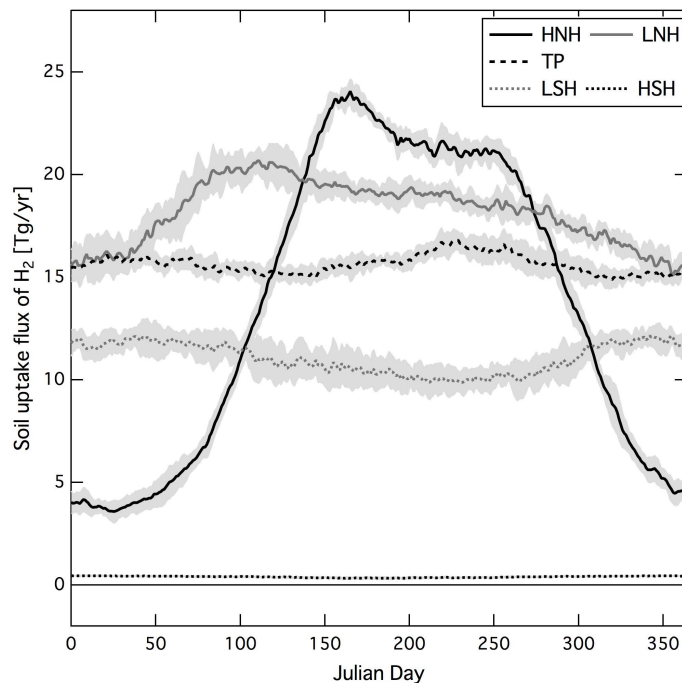
Fig. 2. Seasonal variations of soil uptake flux [Tg/yr] for the latitudinal range of north of 45° N (HNH), 45° N to 15° N (LNH), 15° N to 15° S (TP), 15° S to 45° S (LSH), and the south of 45° S (HSH). Shaded area is the standard deviation of multi-year average, which indicates both the day-to-day variation and inter-annual variation of the flux.
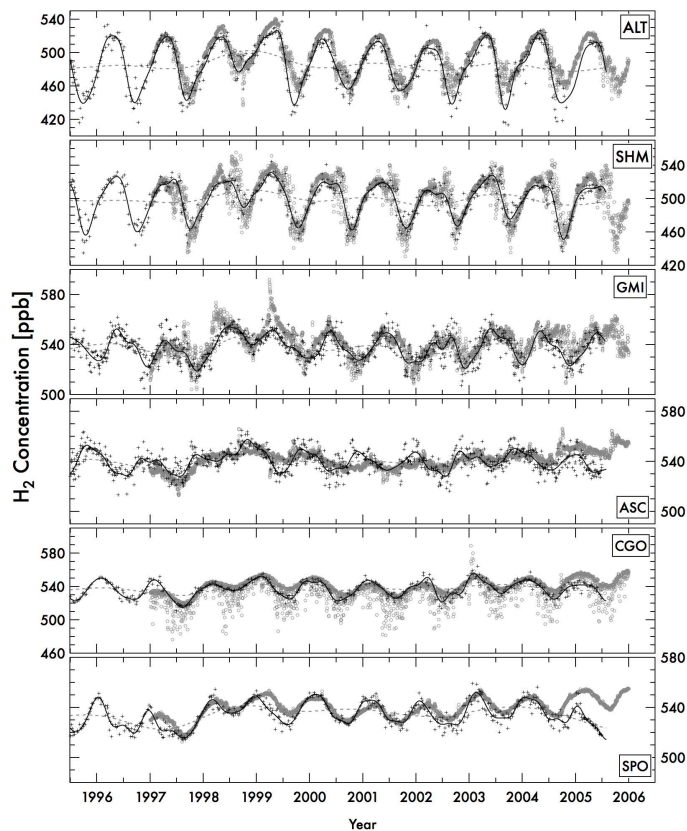
Fig. 3a. H$_2$ concentrations at selected observation sites; ALT(82.5° N), SHM(52.7° N), GMI(13.4° N), ASC(7.9° S), CGO(40.7° S), and SPO(90.0° S). Abbreviation of each site is expressed in Table 1. Cross marks are the observed values, solid lines are the best fit curves to the data, dashed lines are the long-term trends, and gray open circles are the values calculated using the CHASER model.
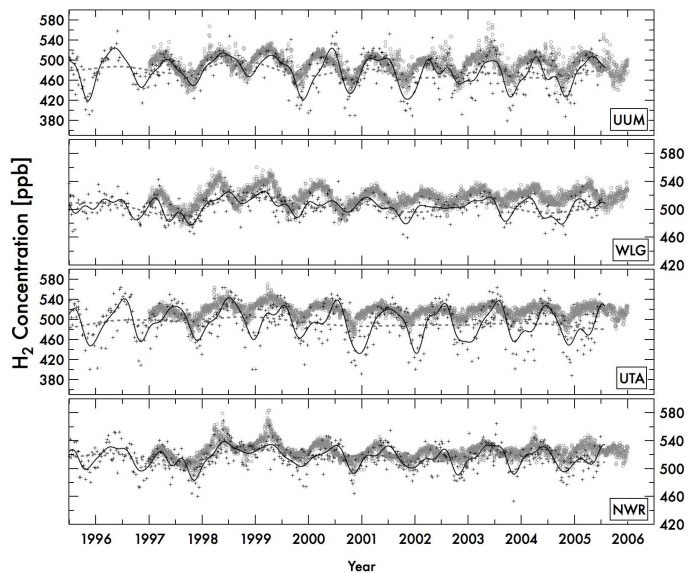
Fig. 3b. Same as Fig. 3a, but for UUM(44.5° N), WLG(36.3° N, 3810 m), UTA(39.9° N), NWR (40.0° N, 3523 m).

ACPD

11, 4059–4103, 2011

Chemical transport model simulation

H. Yashiro et al.

Title Page

| Abstract | Introduction |

| Conclusions | References |

| Tables | Figures |

◀ ▶

◀ ▶

| Back | Close |

Full Screen / Esc

Printer-friendly Version

Interactive Discussion
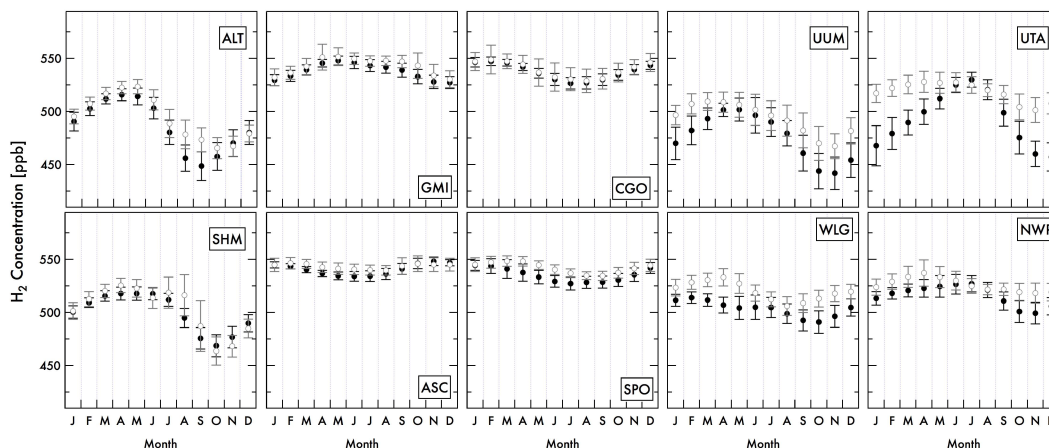
Fig. 4. Monthly mean H_2 concentrations at selected 10 observation sites. Abbreviation of each site is expressed in Table 1. Closed and open circles are the observed and calculated values, respectively. Error bars represent the standard deviations of the multi-year average during the period 1997–2005, which indicates both the day-to-day variation and inter-annual variation of the concentration.
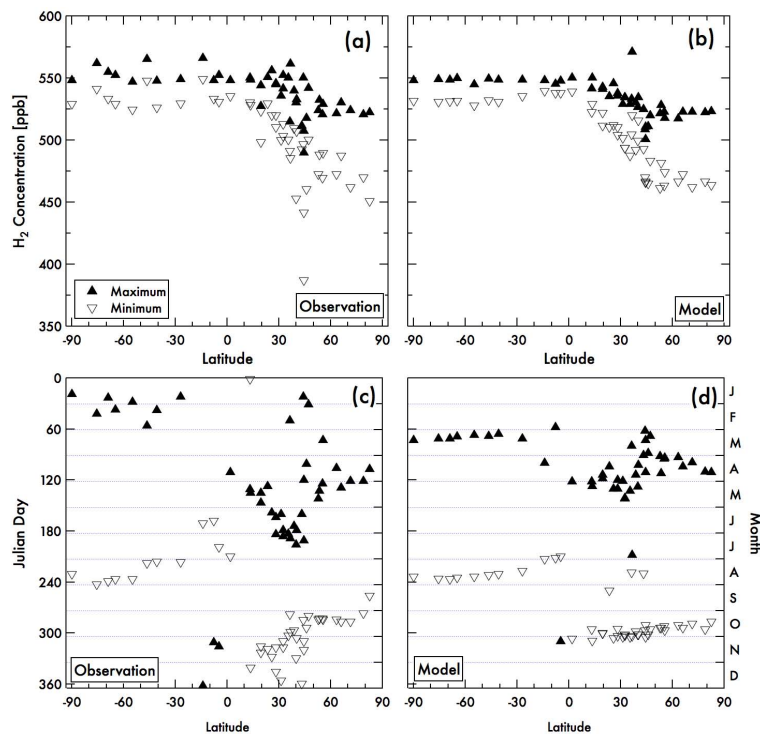
Fig. 5. Latitudinal distribution of seasonal maximum (closed triangle) and minimum (open triangle) for H$_2$ concentration (upper panel, **a, b**) and for occurrence date (lower panel, **c, d**). The values obtained from the observations **(a, c)** and model simulation **(b, d)**.
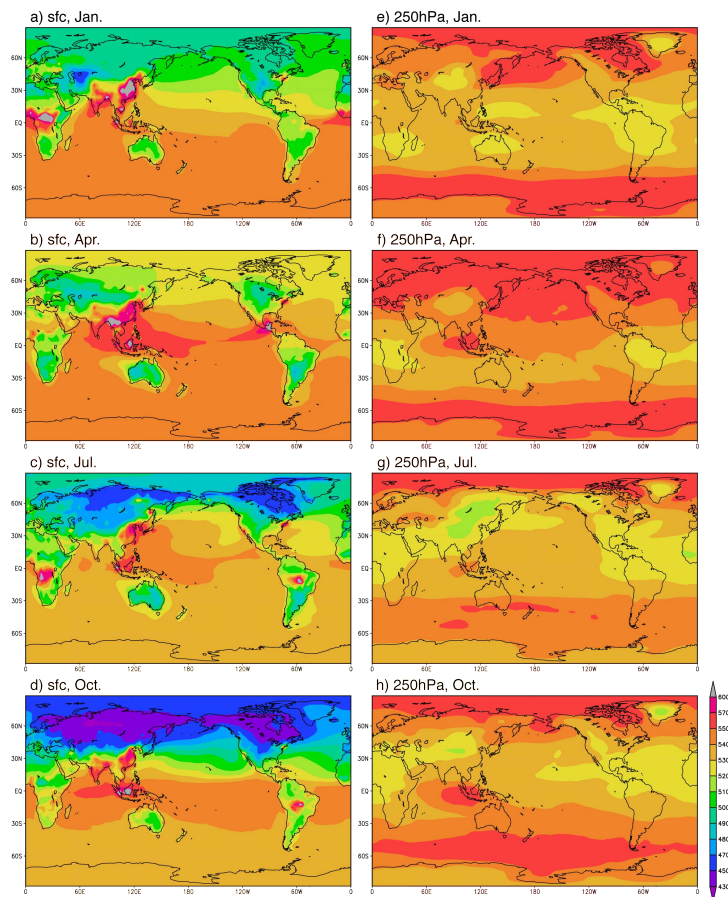
Fig. 6. Distribution of H$_2$ concentration (ppb) calculated at the surface (left panel) and 250 hPa (right panel) for January **(a, e)**, April **(b, f)**, July **(c, g)**, October **(d, h)**. The values are averaged during the period of 1997–2005.
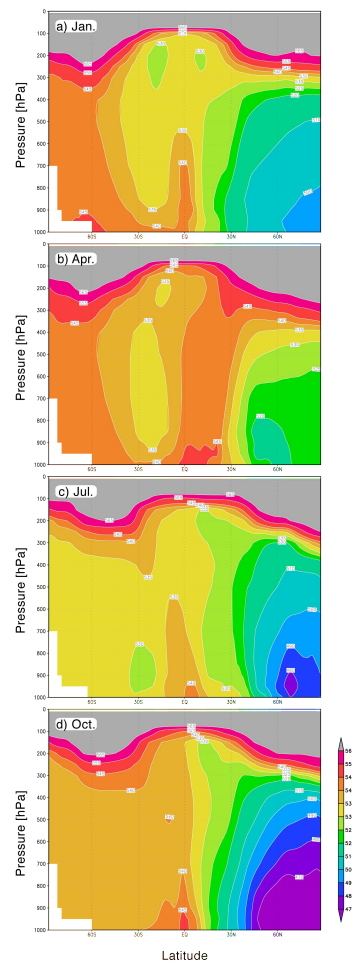
Fig. 7. Latitude-pressure cross-section of zonally averaged H$_2$ concentration (ppb) calculated for January **(a)**, April **(b)**, July **(c)**, October **(d)**. The values are averaged during the period 1997–2005.
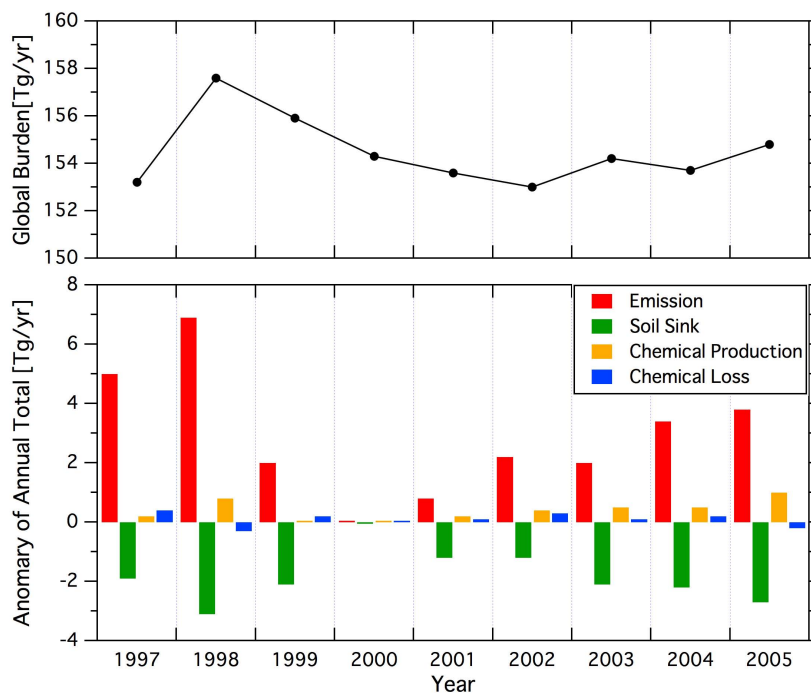
Fig. 8. Global annual averages of the sources and sinks of H_2 (lower panel) and global burden of H_2 (upper panel) during the period 1997–2005. Four budget terms are expressed with the anomaly from 2000, respectively, and the total of them in 2000 is $-3.9\,\mathrm{Tg\,yr^{-1}}$.
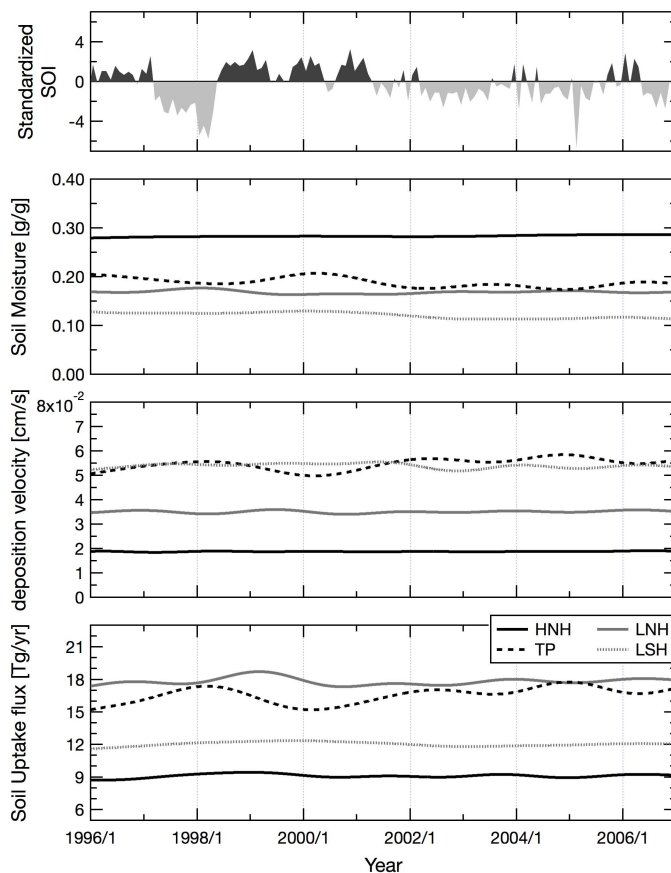
Fig. 9. Long-term trends of soil uptake flux, deposition velocity, and soil moisture for the four latitudinal bands. The latitudinal ranges of HNH, LNH, TP, and LSH are same as Fig. 2. Normarized Southern Oscillation Index (SOI) by Ropellewski and Halpert (1987) is also shown.

Title Page

Abstract | Introduction

Conclusions | References

Tables | Figures

|◄ | ►|

◄ | ►

Back | Close

Full Screen / Esc

Printer-friendly Version

Interactive Discussion
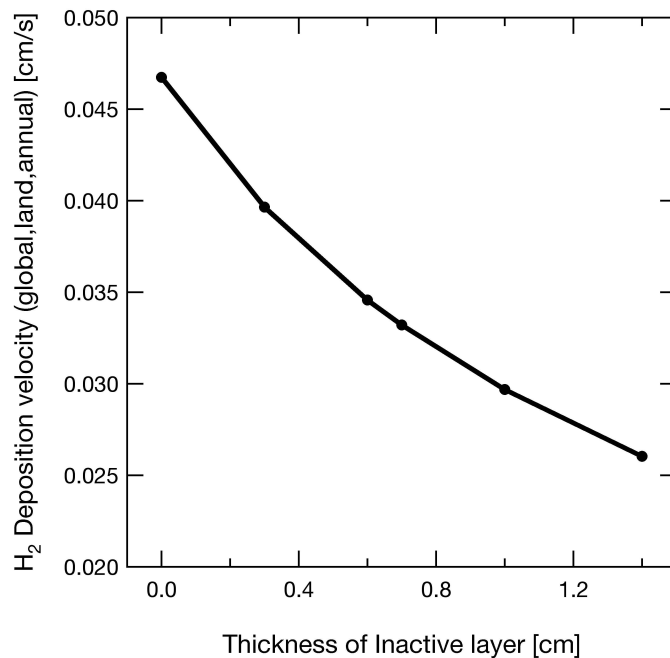
Fig. 10. Sensitivity experiments for change in the global averaged H_2 deposition velocity on land as a function of the thickness of inactive layer.

Title Page

Abstract | Introduction

Conclusions | References

Tables | Figures

◄ | ►

◄ | ►

Back | Close

Full Screen / Esc

Printer-friendly Version

Interactive Discussion